Evidence for deeply-subducted lower-plate seamounts at the Hikurangi subduction margin: implications for seismic and aseismic behavior

Bryant Chow[1], Yoshihiro Kaneko[2], and John Townend[1]

[1]Victoria University of Wellington
[2]Kyoto University

November 22, 2022

Abstract

Seamounts are found at many global subduction zones and act as seafloor heterogeneities that affect slip behavior on megathrusts. At the Hikurangi subduction zone offshore the North Island, New Zealand, seamounts have been identified on the incoming Pacific plate and below the accretionary prism, but there is little concrete evidence for seamounts subducted past the present day coastline. Using a high-resolution, adjoint tomography-derived velocity model of the North Islan, New Zealand we identify two high-velocity anomalies below the East Coast and an intraslab low-velocity zone up-dip of one of these anomalies. We interpret the high-velocity anomalies as two previously-unidentified, deeply-subducted seamounts, and the low-velocity zone as fluid in the subducting slab. The seamounts are inferred to be 10–30km wide and on the plate interface at 12–15km depth. Resolution analysis using point spread functions confirm that these are well-resolved features. The locations of the two seamounts correlate with bathymetric features whose geometries are consistent with those predicted from analog seamount subduction experiments. The spatial characteristics of seismicity and slow slip events near the inferred seamounts agree well with previous finite element modeling predictions on the effects of seamount subduction on megathrust stress and slip. Anomalous geophysical signatures, magnetic anomalies, and swarm seismicity have also been observed previously at one or both seamount locations. We propose that permanent fracturing of the northern Hikurangi upper plate by repeated seamount subduction may be responsible for the dichotomous geodetic behavior observed, and partly responsible for along-strike variations in plate coupling on the Hikurangi subduction interface.

Evidence for deeply-subducted lower-plate seamounts at the Hikurangi subduction margin: implications for seismic and aseismic behavior

Bryant Chow [1,2], Yoshihiro Kaneko [3], John Townend [1]

[1]School of Geography, Environment and Earth Sciences, Victoria University of Wellington
[2]GNS Science
[3]Department of Geophysics, Kyoto University

Key Points:

- We image velocity anomalies below the North Island, New Zealand, interpreted as deeply-subducted seamounts and fluid in the downgoing plate
- Independent geological and geophysical observations corroborate our seamount interpretation
- Inferred seamounts and intraslab fluid may partly explain enigmatic, along-strike plate-coupling transition at the Hikurangi margin

Corresponding author: Bryant Chow, `bryant.chow@vuw.ac.nz`

Abstract

Seamounts are found at many global subduction zones and act as seafloor heterogeneities that affect slip behavior on megathrusts. At the Hikurangi subduction zone offshore the North Island, New Zealand, seamounts have been identified on the incoming Pacific plate and below the accretionary prism, but there is little concrete evidence for seamounts subducted past the present day coastline. Using a high-resolution, adjoint tomography-derived velocity model of the North Islan, New Zealand we identify two high-velocity anomalies below the East Coast and an intraslab low-velocity zone up-dip of one of these anomalies. We interpret the high-velocity anomalies as two previously-unidentified, deeply-subducted seamounts, and the low-velocity zone as fluid in the subducting slab. The seamounts are inferred to be 10–30km wide and on the plate interface at 12–15km depth. Resolution analysis using point spread functions confirm that these are well-resolved features. The locations of the two seamounts correlate with bathymetric features whose geometries are consistent with those predicted from analog seamount subduction experiments. The spatial characteristics of seismicity and slow slip events near the inferred seamounts agree well with previous finite element modeling predictions on the effects of seamount subduction on megathrust stress and slip. Anomalous geophysical signatures, magnetic anomalies, and swarm seismicity have also been observed previously at one or both seamount locations. We propose that permanent fracturing of the northern Hikurangi upper plate by repeated seamount subduction may be responsible for the dichotomous geodetic behavior observed, and partly responsible for along-strike variations in plate coupling on the Hikurangi subduction interface.

Plain Language Summary

Seamounts are large volcanic edifices on the seafloor that eventually make their way into subduction zones. Seamounts have been identified at various stages of subduction and are thought to either promote or suppress the occurrence of large earthquakes at subduction zones. It is difficult to track seamounts far into a subduction zone due to the decreasing sensitivity of most geophysical measurements with increasing depth. In this study, we identify several distinctive seismic velocity anomalies in a high-resolution 3D model of the North Island, New Zealand. The model is derived using a form of seismic imaging that improves fits between observed and simulated seismic waveforms. We interpret the anomalies to indicate the presence of two deeply-subducted seamounts and fluid in the downgoing plate. The two seamounts are inferred to be at interface depths, with horizontal dimensions of about 10-30km. These features are well resolved and our interpretations are supported by independent evidence including seafloor bathymetry data and the presence of nearby geophysical anomalies. We associate these seamounts with variations in slip behavior observed along the Hikurangi subduction margin and propose that they have caused permanent damage to the upper plate, thereby reducing its ability to store energy and produce large earthquakes.

1 Introduction

Seamounts are prominent seafloor features found globally at convergent margins, where their eventual subduction has been observed to have significant effect on upper plate morphology, and is predicted to influence megathrust slip behaviour. While shallow subduction of partially buried seamounts has been inferred to play a role in tectonic erosion and deformation of the upper plate (e.g., Dominguez et al., 1998; Von Huene & Scholl, 1991), less is known about what happens as a seamount subducts further because of the limited resolution of geophysical methods commonly used to identify subducting seamounts. Previous studies have imaged buried seamounts at shallow stages of subduction (e.g., Bangs et al., 2006; Pedley et al., 2010; Marcaillou et al., 2016; Frederik et al.,

2020) and, in more limited cases, deeper into subduction zones (e.g., Kodaira et al., 2000; Singh et al., 2011).

Arguments linking subducted seamounts to large-earthquake seismogenesis are at first glance discordant, suggesting either that seamounts facilitate seismic rupture by acting as locally locked asperities on which large earthquakes can nucleate (Scholz & Small, 1997), or that they impede seismic rupture by fracturing the upper plate and rendering it incapable of storing sufficient elastic strain to produce large earthquakes (Wang & Bilek, 2011). A number of ideas have been proposed regarding the effects of seamounts on mechanical and hydrological processes in the upper plate, which may explain how subducted seamounts promote both seismic and aseismic behavior (Sun et al., 2020), allow for the subduction and compaction of additional sediments to depth (Ellis et al., 2015), act as rupture barriers for large earthquakes (Yang et al., 2013), and transport inordinate amounts of fluid into subduction zones (Bell et al., 2010; Chesley et al., 2021). However, the small number of documented examples of deep seamount subduction makes it difficult to resolve the complex relationship between seamounts and slip behavior at subduction zones.

In Chow et al. (companion manuscript) we use adjoint tomography, an imaging technique that involves fitting short-period (> 4 s) earthquake-generated seismic waveforms to corresponding synthetic waveforms, to refine a 3D velocity model of the North Island of New Zealand (Eberhart-Phillips et al., 2020). Throughout the inversion, strong velocity anomalies in the forearc region are imaged at increasing resolution. Two high-velocity anomalies are resolved as point-like structures, spanning tens of km, with peaked amplitudes at plate interface depths. We also observe a broad low-velocity zone up-dip of one of these anomalies. Here, we (1) assess the robustness of those velocity anomalies in more detail, (2) interpret them as prominent tectonic features using corroborating geophysical and geological evidence, and (3) discuss the implications of such features for seismic and aseismic behavior at the Hikurangi subduction zone.

2 Hikurangi subduction zone

The Hikurangi subduction zone is a convergent plate boundary where the Pacific plate is subducting obliquely westward beneath the Australian plate (Figure 1). The Hikurangi margin exhibits varying differences in along-strike properties (Wallace et al., 2009), and is commonly separated into northern, central, and southern margins (Figure 1). The northern section of the margin is characterized by thin incoming sediment cover, a relatively high convergence rate (~ 50 km/yr), and tectonic erosion of the frontal wedge from repeated seamount subduction, resulting in a steep and narrow accretionary wedge (20–40 km). Conversely, the central and southern segments exhibit thicker incoming sediment cover (> 5 km), slower (20–40 mm/yr) and increasingly oblique convergence, and a well-developed, broad, shallow-tapered accretionary wedge (30–70 km) (Barnes et al., 2010; Wallace, 2020). Although relative plate motion at the Hikurangi subduction zone is oblique (and increases in obliquity southward), much of the rotational component is accommodated by right-lateral strike-slip faults in the overlying crust of the North Island (Beanland & Haines, 1998; Wallace et al., 2004, 2009). This has the effect that plate convergence rates at crustal depths are primarily margin-normal at the trench, with decreasing convergence rates from north to south (Figure 2).

The incoming seafloor at the northern Hikurangi margin (i.e., north of latitude S40°) is strewn with seamounts at various stages of subduction. Sediment cover here is relatively thin, and consequently numerous knolls and seamounts are identifiable in high-resolution bathymetry (Figure 1). Seamounts subducted beneath the accretionary pile have been imaged using marine seismic reflection surveys (e.g., Barker et al., 2009; Barnes et al., 2010; Bell et al., 2010). These seamounts are associated with localized uplift of the seafloor and localized positive magnetic anomalies, and are preceded landward by high-reflectively zones interpreted to represent underthrust sediment packages (Bell et al., 2010; Ellis et al., 2015). The identified seamounts are typically oblate in shape with estimated footprints on the scale of tens of kilometers, and heights of less than a few kilometers (Barnes et al., 2010; Bell et al., 2010). Although no seamounts subducted further below the North Island have been identified through geophysical methods, some have been inferred by other means. For example, tectonic reconstructions based on the Poverty and Ruatoria Re-entrants suggest that very large seamounts have been subducted hundreds of kilometers westward beyond the trench and may currently reside somewhere below the northern North Island (Figure 1; K. B. Lewis et al., 1998; Pedley et al., 2010).

The Hikurangi margin presents a rare opportunity to study an active subduction zone with land-based measurements. The subducting Pacific plate is part of a large igneous province, the Hikurangi plateau, and subduction of this relatively buoyant feature has caused much of the forearc region to become subaerial (Litchfield et al., 2007; Nicol et al., 2007). Consequently, the plate interface below the East Coast region is shallow at 12–15 km depth (Figure 2; Williams et al., 2013). Geodetic inversions used to infer plate coupling along the interface suggest that the southern Hikurangi margin is geodetically locked, while the northern portion is creeping aseismically (Figure 2; Wallace, Beavan, et al., 2012; Wallace, 2020). The transition between the two styles of slip occurs across the central margin (Figure 2) with shallow (5–15 km) slow slip events (SSEs) at the northern margin accommodating the majority of expected plate motion where they occur (Figure 2; Wallace, 2020). The cause of along-strike differences at the Hikurangi margin is an ongoing topic of research, and a variety of factors including fluids, seamounts, overriding plate structure, incoming sediment flux, and temperature have been suggested as explanations for the heterogeneous slip behavior observed (Wallace, 2020).

3 Data and methods

In Chow et al. (companion manuscript) we use earthquake-based adjoint tomography to image crustal structure with kilometer-scale resolution at the Hikurangi subduction zone. In adjoint tomography, the misfit between earthquake-generated seismic waveforms and corresponding wave propagation simulations is minimized in an optimization problem. Seismic velocities are iteratively perturbed to reduce this data–synthetic misfit and improve on an initial velocity model, which in our work is a ray-based 3D tomography model of New Zealand (Eberhart-Phillips et al., 2020). The inversion dataset consists of 60 geographically well-distributed earthquakes, whose waveforms were recorded at as many as 88 broadband seismometer locations (Figure 1). The total dataset consists of approximately 1800 unique source–receiver pairs. Observed and synthetic waveforms are compared using a cross-correlation traveltime misfit at waveform periods of 4–30 s. Adjoint methods are used to derive the gradient of the misfit function, and an inverse L-BFGS Hessian and backtracking line search are applied to obtain a search direction and step length (Modrak & Tromp, 2016; Chow et al., 2020). In total, 28 iterations are performed, resulting in velocity changes of as much as $\pm 30\%$ with respect to initial values. The final velocity model is assessed using point spread functions (Fichtner & Trampert, 2011) and comparisons with known tectonic and geologic features of New Zealand. In this study, we focus explicitly on velocity anomalies identified in the forearc region of the velocity model. Further elaboration on the inversion and interpretations of the velocity model as a whole can be found in Chow et al. (companion manuscript).

4 Results

4.1 East Coast velocity anomalies

We identify two high-velocity anomalies below the East Coast and a deep offshore low-velocity zone (Figure 3). The high-velocity anomalies are located at approximately plate interface depths ($\sim$12–15 km), below Māhia Peninsula (Feature M; Figure 3) and the North Island township of Pōrangahau (Feature P; Figure 3). The low-velocity zone is located seaward of the Pōrangahau anomaly (Feature O; Figure 3). As shown in Figure 5 of Chow et al. (companion manuscript), these anomalies emerge early in the inversion process, suggesting that they are required to reduce long-period data–synthetic misfit. Visualized using a 12 km depth slice through the velocity model (Figure 3A), the high-velocity anomalies appear circular with V_s>3.5 km/s.

The two high-velocity anomalies are distinct with respect to the surrounding velocity structure. In cross-section, they are characterized by bumps of high velocities (V_s>3.25 km/s) centered at interface depths (Figure 3B, C). The anomaly below Māhia Peninsula shows a broad region of elevated velocities extending to 20 km depth, almost 10 km below the assumed plate interface ($\sim$ 12 km). Above the interface, increased velocities can be seen extending to shallow depths ($\sim$5 km; Figure 3B). The Pōrangahau anomaly has a smaller relative lateral extent, and a more pronounced expression of high velocities extending upwards to the surface (Figure 3C) and below the subduction interface. A distinctive difference of the Pōrangahau anomaly is a systematic dip in seismic velocities further seaward, corresponding to the offshore low-velocity zone (Feature O). The two high-velocity anomalies have similar geometries in a trench-parallel cross-section (Figure 3D).

The ratio of seismic velocities (V_p/V_s) is often used to infer the presence of fluids at depth. Due to the higher sensitivity of V_s to the presence of fluids, low V_p/V_s values are commonly used to indicate low fluid content, and vice versa (Christensen, 1996; Ito et al., 1979; Eberhart-Phillips et al., 1989, 2005; Audet et al., 2009). For a Poisson solid (Poisson's ratio= 0.25), the V_p/V_s ratio is equal to 1.73: we use the Poisson's solid as our reference to define high (>1.73) and low (<1.73) V_p/V_s ratios. The two high-velocity anomalies are characterized by low V_p/V_s values (<1.6) surrounded by higher V_p/V_s (>1.8; Figure 4), suggesting lower fluid content compared to the surrounding accretionary prism. The offshore low-velocity zone is more marked, appearing as a high-V_p/V_s feature (>2) adjacent to the Pōrangahau anomaly and coincident with a region of frequent (every 4–5 years) slow slip events (Figure 2; Wallace, 2020). This high-V_p/V_s feature is columnar in shape, extending through the entire 30 km depth range illustrated, suggesting that it may be associated with a source in the subducted oceanic crust.

4.2 Resolution analysis

Point spread functions (PSFs) provide a measure of how point-like perturbations are blurred or smeared by an inversion (Fichtner & Trampert, 2011), and have seen extensive use as resolution tests in adjoint tomography studies (e.g Zhu et al., 2015; Bozdağ et al., 2016; Tao et al., 2018). To perform point spread tests, we perturb our final velocity model $\mathbf{m}$ by a quantity $\delta\mathbf{m}$, and attempt to recover the perturbation by solving for the action of the Hessian on the model perturbation (Fichtner & Trampert, 2011). In practice, this is accomplished using finite-differences of gradients

$$\mathbf{H}(\mathbf{m})\delta\mathbf{m} \approx \mathbf{g}(\mathbf{m}+\delta\mathbf{m}) - \mathbf{g}(\mathbf{m}), \tag{1}$$

where $\mathbf{H}(\mathbf{m})$ is the Hessian evaluated at the final model $\mathbf{m}$, $\mathbf{g}(\mathbf{m})$ is the gradient evaluated at the final model, and $\delta\mathbf{m}$ is a local model perturbation with respect to the final model. The resulting quantity $\mathbf{H}(\mathbf{m})\delta\mathbf{m}$ is a conservative estimate of the PSF, which provides practical information on the extent of how features in the tomographic model can be interpreted (Fichtner & Trampert, 2011). Individual point spread tests define $\delta\mathbf{m}$ as a 3D spheroidal Gaussian with peak amplitude equal to 15% of the final V_s model. The size and location of the perturbations are chosen to reflect the individual velocity anomaly being probed. We perform four individual point spread tests to understand the resolution of the anomalies identified in Section 4.1.

In Chow et al. (companion manuscript) we also calculate the Fourier transform of the Hessian at zero wavenumber, or zeroth moment, which conveys how resolution of the underlying dataset varies across the model domain. The zeroth moment test recovers a homogeneous volumetric perturbation in place of $\delta\mathbf{m}$ (Fichtner & Trampert, 2011). In similar fashion to a ray coverage plot, the zeroth moment shows how resolution varies relatively, but does not provide information on resolution length. Depth slices through the zeroth moment volume are shown in Figure A1, using a threshold value chosen to represent the lateral extent of sensitivity in our velocity model. The threshold region contains all three velocity anomalies to depths of 25 km, meaning our dataset is sensitive to velocity heterogeneities in these regions. The pink shaded areas in Figures 3 and 4 show the same threshold value in which the updated velocity model is interpretable.

The PSF for the Māhia Peninsula anomaly has a complicated geometry (Feature M; Figure 5A, C). The peak of the PSF lies a few kilometers offshore from the perturbation itself, indicating uncertainty of a few kilometers in deriving an exact location (Figure 5A). Similarly, lateral smearing over ∼100 km suggests that the size of the heterogeneity is not well constrained and that the actual heterogeneity could be smaller than the corresponding velocity signature. Interestingly, the PSF contains a second peak further inland, and a high-amplitude feature to the south, indicating that the updated velocity structure at these locations is affected by heterogeneity beneath the Peninsula. The model shows no corresponding high-velocity anomalies at these locations however (Figure 3), suggesting that this trade-off does not significantly impact the final velocity model. Vertical smearing (Figure 5C) indicates that the heterogeneity affects the inferred velocity structure above and below itself, which likely explains the large vertical extent seen in the V_s and V_p/V_s models (Figures 3, 4).

The PSF for the Pōrangahau anomaly (Feature P; Figure 4) shows that the heterogeneity here is more well-resolved, with location uncertainty of a few kilometers (Figure 5B). The PSF also indicates that there is minimal trade-off with the surrounding velocity structure, but lateral smearing means that the width of the velocity anomaly may be larger than the actual heterogeneity. In cross-section (Figure 5D), the peak of the PSF is located a few kilometers above the input perturbation. This may explain the apparent shallow, mid-crustal depth of the Pōrangahau anomaly (Figure 4C), which may be an artefact of the inversion. Conversely, this suggests that the true heterogeneity is likely situated deeper than the corresponding velocity anomaly, and that the shallow, vertically-elongated velocity structure is a result of vertical smearing (Figure 5D).

We perform two additional point spread tests to assess the resolution of the offshore low-velocity anomaly (Feature O; Figure 4). The first test attempts to recover a low-velocity anomaly within the subducting slab (Figure 5E). The resulting PSF shows a columnar structure, similar to that observed in V_p/V_s (Figure 4C). To ensure that this columnar structure could not also be the result of a velocity anomaly in the upper plate, we perform a similar test for a low-velocity anomaly input above the plate interface (Figure 5F). The resulting PSF shows that recovery is primarily confined to the upper plate, and consequently implies that the presence of an upper-plate, low-velocity feature would not explain the offshore low-velocity anomaly imaged. In other words, the heterogeneity (Feature O; Figure 4) is likely an intra-slab low-velocity (high-V_p/V_s) anomaly, whose signature is smeared considerably in the vertical direction (Figure 4C).

Overall, the point spread tests performed for the East Coast velocity anomalies suggest that: (1) the lateral locations of the anomalies are well resolved, with spatial uncertainties less than ten kilometers; (2) the lateral extent of the features is affected by smearing, but may be roughly estimated by measuring the width of the peak amplitudes of the velocity anomalies; and (3) the vertical extent and exact depths of the features are not well-constrained but the two high-velocity anomalies are likely at interface depths and the low-velocity and high-V_p/V_s offshore anomaly is located within the subducting slab.

4.3 Isosurface visualization

Isosurfaces represent points of constant value within a volume of space and are a useful tool for highlighting structures within three-dimensional models. To better visualize the high-velocity anomalies below the East Coast we investigated various velocity isosurfaces using our V_s velocity model. The selected isosurface defines a constant V_s=3 km/s with vertically exagerrated points colored by depth (Figure 6A). The isosurface is rotated to an oblique, trench-perpendicular viewing angle so that both velocity anomalies are clearly visible.

We choose the value of the isosurface (V_s=3 km/s) to highlight the most prominent segments of the high-velocity anomalies discussed previously, identifiable as yellow colors in Figure 3B–D. In terms of tectonic structure, this process can be thought of as the stripping away of low-velocity sediments overlying stiffer material such as oceanic and continental crust. This effect is clearly visible in the isosurface as removal of the sedimentary and volcanic cover on the Australian plate and the adjacent accretionary wedge (Figure 6A; Edbrooke et al., 2015). The remaining structures are likely related to basement rocks of the North and South Islands (Mortimer, 2004) and the backstop of the subduction zone forearc (Byrne et al., 1993).

Clearly identifiable in the isosurface are two solitary peaks related to the high-velocity anomalies below Pōrangahau and Māhia Peninsula. Similar to the 2D cross-sections (Figure 3B–D), the Pōrangahau anomaly is a tall, narrow peak that extends to the surface, while the Māhia Peninsula anomaly features a wide base and lower relative height. Further seaward a third prominent peak is visible, which spatially correlates with Rock Garden, a known seamount on the incoming Pacific plate (Barnes et al., 2010). Other sections of the isosurface can be linked to known tectonic features of New Zealand. These include a notch in the backstop related to Cook Strait (K. B. Lewis et al., 1994), deep depressions related to Taranaki basin (e.g., King & Thrasher, 1996) and Whanganui basin (e.g., Carter & Naish, 1998), and a collection of shallow depressions throughout the Taupō Volcanic Zone (Wilson et al., 1995, 2009). These tectonic features are discussed in more detail in Chow et al. (companion manuscript).

5 Discussion

5.1 Deeply subducted seamounts below the East Coast

We interpret the East Coast high-velocity anomalies as previously-unidentified deeply-subducted seamounts located below Pōrangahau and Māhia Peninsula (Figure 1). The 3 km/s isosurface of the velocity model highlights these features, and their apparent effect on the velocity structure of the upper crust, remarkably well (Figure 6A). We can estimate the size and depth of the two seamounts, but note that depending on their actual shape and aspect ratio their full extent may fall below the resolution limit of the tomographic inversion. In other words, the lateral width of the seamounts could be larger than the corresponding velocity signature.

Subduction of partially buried seamounts would have an observable effect on the structure of the accretionary prism and the upper plate, which can be corroborated with known geologic features. Sand table experiments and field observations have been used to predict the effects of subducted seamounts on the upper plate, which include: tectonic erosion at the frontal wedge leading to re-entrant bathymetric features, a complex fracture network that forms in the vicinity of the seamount and is preserved as a permanent furrow or scar, local uplift above the seamount, and increased subsidence in the seamount's wake (Figure 6B; Dominguez et al., 1998, 2000).

5.1.1 Māhia Peninsula seamount

We propose that a large seamount has been subducted below Māhia Peninsula. We estimate the extent of this Māhia Peninsula seamount at 25 km based on its V_p/V_s signature. A seamount attached to the incoming plate would sit at plate interface depth, which is at approximately 12 km depth (Williams et al., 2013). In this section we present external evidence that corroborates our interpretation.

The Poverty Re-entrant northeast of Māhia Peninsula has been interpreted as a seamount scar resulting from consecutive seamount impacts over the last 1–2 Myr (Figure 6C; K. Lewis & Pettinga, 1993; Collot et al., 1996; K. B. Lewis et al., 1998; Pedley et al., 2010). Based on relative locations and the plate convergence direction, it is likely this re-entrant is associated with the Māhia Peninsula seamount. The Poverty Re-entrant has previously been identified as a double feature consisting of lower and upper indentations (Collot et al., 1996). The geometry of the lower indentation (i.e. steep-sided, "V"-shaped deflection of the frontal wedge) is suggestive of a re-entrant, while the morphology of the upper indentation indicates eastward subsidence and subsequent canyon erosion (Collot et al., 1996). The upper Poverty indentation has been linked to subsidence and drainage development in the wake of a very large seamount (Pedley et al., 2010), which we propose may be the Māhia Peninsula seamount imaged here. Topographic uplift would similarly be expected for a seamount below land, and may explain the anomalous topographic high of Māhia Peninsula with respect to the surrounding coastline (Figure 6C).

Other studies have inferred the presence of a deeply subducted seamount near Māhia Peninsula. The offshore Lachlan fault system (Figure 1) has undergone almost 6 km vertical separation of its northern segment with respect to its southern extent, which Barnes et al. (2002) hypothesized to be the upper-plate response to a subducted seamount >10 km below the Peninsula. Approximately 20 km landward of Māhia Peninsula, the Mōrere thermal spring is one of only two thermal springs in this region, whose chemical signature show enrichment in mantle components suggesting that high-permeability paths extend from the subducted plate to the surface (Figure 1; Reyes et al., 2010). The coincident Mōrere magnetic anomaly has been linked to a seamount subducted within the last 2 Myr (+70 nT; Hunt & Glover, 1995), which agrees with previous associations of positive magnetic anomalies with locations of offshore seamounts (Bell et al., 2010).

Below the Mōrere thermal spring, ray-based tomography revealed a high-V_p anomaly at approximately 8 km depth, which was suggested to be volcanic in origin (Eberhart-Phillips et al., 2015). Magnetotelluric studies here show a conductive patch on the plate interface, with a more resistive patch below the Peninsula (Heise et al., 2017). The conductive patch was interpreted to indicate the presence of fluid- or clay-rich sediments, and may be related to underthrust, fluid rich sediments at the leading flank of the seamount, similar to those proposed for offshore seamounts at the northern Hikurangi margin (Bell et al., 2010). The Mōrere anomalies may thus correspond to the down-dip extent of the seamount below Māhia Peninsula, as well as the upper crust response to such a geometric heterogeneity.

5.1.2 Pōrangahau seamount

We propose that a previously unrecognised seamount has been subducted almost 100 km beyond the trench and now lies below the East Coast township of Pōrangahau. From the V_p/V_s signature (Figure 4) this inferred Pōrangahau seamount has an approximate lateral extent of 15 km. The seamount is inferred to lie at a plate interface depth of 15 km (Williams et al., 2013).

A distinctive bathymetric feature in the vicinity of the Pōrangahau seamount is Madden Canyon. Although it is too far from the trench ($\sim$ 100 km) to be easily explained as a re-entrant, Madden Canyon may have formed as an area of subsidence in which mass sliding and canyon erosion was promoted at the trailing flank of the Pōrangahau seamount (Figure 6C; Dominguez et al., 1998). There is no obvious re-entrant feature in the bathymetry data related to the Pōrangahau seamount (Figure 6C), but rapid growth of the accretionary pile at the central Hikurangi margin may have obscured such a feature (Von Huene & Scholl, 1991). Similarly, there is no corresponding topographic high, like that represented by Māhia Peninsula, which may indicate that the Pōrangahau seamount lies at a deeper interface depth or is smaller (or both) than the Māhia Peninsula seamount.

Evidence corroborating the presence of the Pōrangahau seamount is limited, which may in part reflect a lack of targeted geophysical studies in this region. The contrast in evidence between the Pōrangahau and Māhia Peninsula seamounts could also be explained by the ages of the two seamounts. A back-of-the-envelope calculation based on a margin normal convergence rate of 39 mm/yr (Figure 2; Wallace, 2020) and distance to the trench of 150 km (Figure 1), suggests that the Pōrangahau seamount first impacted the trench at $\sim$4 Ma. In contrast, the Māhia Peninsula seamount is thought to have subducted in the last 1–2 Myr (K. B. Lewis et al., 1998; Pedley et al., 2010). This difference may explain the contrast in the velocity signatures of the two seamounts. Other potentially impactful differences between the two inferred seamounts that are not well constrained by our results include: the differing characteristics of the accretionary prism, the size and aspect ratio of each seamount, and their respective burial depths prior to subduction.

5.2 Implications for seismic and aseismic behavior

Seamounts entering the Hikurangi subduction zone have previously been identified in the early stages of subduction. Recognition of the Māhia and Pōrangahau subducted seamounts in this study may help to explain anomalous seismic and aseismic behavior observed up-dip from their respective locations. Mentioned previously, numerous factors have been suggested as explanations for variations in coupling coefficient on the Hikurangi megathrust interface. One such interpretation suggests that permeability variations in North Island terrane blocks results in heterogeneous fluid distribution on the interface, leading to the variations in plate coupling (Reyners et al., 2017). However based on our findings, we suggest that the inferred seamounts at Māhia Peninsula and Pōrangahau may play a more central role in along-strike variations in plate coupling.

A study that used finite element modeling of seamount subduction suggests that sediment overconsolidation on the leading flanks of seamounts results in fracturing of the upper plate and increased tectonic compression and yield strength, favoring the storage of elastic strain and seismic behavior (Sun et al., 2020). In contrast, underconsolidation in the stress shadow of the seamount is predicted to result in increased porosity, decreased tectonic compression, and a preference for aseismic behavior such as slow slip (Figure 7B).

Pōrangahau and Māhia Peninsula are both areas of anomalously high rates of clustered seismicity, which may be manifestations of small-to-moderate sized earthquakes observed at the leading edge of subducted seamounts (Bell et al., 2010). Pōrangahau has seen repeated episodes of moderate-magnitude swarm seismicity (Jacobs et al., 2016), and moderately sized earthquakes accompanying geodetically observed SSEs (Figure 7C; Wallace, Beavan, et al., 2012). At Māhia Peninsula, triggered microseismicity has been temporally correlated with shallow SSEs in the region, clustered near the Peninsula (Figure 7D; Delahaye et al., 2009). The increased seismic activity at these two locations may be linked to the inferred seamounts, but further work is needed to draw connections between faulting mechanisms, earthquake depth, and inferred seamount locations.

Geodetic observations show that the locked-to-creeping transition on the Hikurangi plate interface extends approximately NW–SE through the central Hikurangi margin, perpendidular to the trench axis and almost directly through Pōrangahau (Figure 2; Wallace, 2020). The margin further south is interpreted to be more geometrically and compositionally uniform, enabling broader zones of locking, while to the north shallow slow slip events accommodate a majority of plate motion aseismically (Wallace, 2020). Interestingly, the spatial extent of the shallow northern SSEs is segmented around Hawke Bay, with a southern terminus just south of Pōrangahau (Figure 7A). This segmentation roughly correlates with the locations of the two deeply subducted seamounts and may be linked to the affected upper-plate regions surrounding each seamount (dashed blue circles; Figure 2).

Several theories have been posited to link seamounts with megathrust slip behavior. Based on the locations of our two seamounts in a predominantely aseismic patch of the plate interface (Figure 2), our findings are consistent with the idea put forth by Wang and Bilek (2011) that describes seamounts as geometric irregularities impinging on the upper plate. According to this interpretation, seamounts must break through upper plate rocks to accommodate plate convergence and, at low temperatures corresponding to shallow seismogenic depths, this results in fracturing of the accretionary wedge and upper plate, and to a lesser degree the seamount itself. Between the point at which a seamount initially enters the trench and the depths at which mantle viscosity becomes relevant, these seamounts are expected to damage their surroundings brittlely, leaving a permanent scar in their wake that is less able to accumulate elastic strain necessary for coseismic rupture propagation (Wang & Bilek, 2011; Cummins et al., 2002; Bangs et al., 2006).

We propose that repeated seamount subduction at the northern Hikurangi margin has resulted in a region of extensive upper plate fracturing (Figure 7A). In contrast, any seamounts entering the southern margin are thought to be buried under several kilometers of sediments, which may suppress their effects on upper plate morphology and allow the interface to lock (Figure 7B; Wallace, 2020). This line of argument has previously been unable to account for the location of the locked-to-creeping transition at the central Hikurangi margin, because the central margin features a more well-developed accretionary wedge with respect to the northern margin. This is more consistent with a smooth incoming seafloor and therefore a locked interface (Wallace, 2020), but our recognition of a seamount below Pōrangahau is capable of explaining the location of the locked-to-creeping transition. In other words, the seamount at Pōrangahau may represent the southern extent of partially buried seamounts that are able to significantly influence the mechanical integrity of the upper plate.

The high-V_p/V_s intraslab feature (Figure 4C) identified in this study may also play a role in SSE timing and location. Warren-Smith et al. (2019) proposed that episodic release of fluid pressure from the over pressured subducting crust into the upper plate influences the timing of slow slip events on the megathrust. Our imaged high-V_p/V_s anomaly may be a manifestation of fluids in the subducting slab, and its location below the southern end of a region of repeating SSEs (Figure 7D) appears to agree with the idea that accumulation and release of fluid pressure has an influence on slow slip events (Warren-Smith et al., 2019). The proximity of the inferred fluid source to the Pōrangahau seamount also suggests some link. Seamount subduction modeling suggests that aseismic slip should be the preferred behavior at the trailing flank of a subducted seamount (Figure 7B; Sun et al., 2020), but further work is needed to draw firm connections between fluids in the downgoing slab, shallow slow slip events, and subducted seamounts.

6 Conclusions

We identify velocity anomalies below the east coast of the North Island of New Zealand using a newly-derived adjoint tomography velocity model. Point spread functions are used to constrain the robustness of these features, showing that they are well resolved, although smearing in the inversion procedure increases the uncertainty of their sizes and shapes.

The two high-velocity anomalies are interpreted as previously-unidentified, deeply-subducted seamounts below Māhia Peninsula and Pōrangahau, and a distinctive low-velocity (high-V_p/V_s) anomaly corresponding to an intraslab fluid source. The approximate size and location of the two seamounts are consistent with those of known offshore seamounts, and with the existence of bathymetric features predicted by analog sand table experiments. We propose the Poverty Re-entrant to be both the re-entrant and associated subsidence feature related to subduction of the Māhia Peninsula seamount. The anomalous topographic high of the Peninsula is also linked to predicted topographic uplift above the inferred seamount. We propose that Madden Canyon is a corresponding subsidence feature related to the Pōranghau seamount, which first impacted the trench ~ 4 Ma, based on modern plate convergence rates. We suggest that corresponding evidence such as a re-entrant or topographic uplift may be obscured due to the relative age, size, or location of the seamount relative to the Māhia Peninsula seamount.

Anomalous seismic and geodetic phenomena observed at Pōranghau and Māhia Peninsula — including swarm seismicity, magnetic anomalies, and a solitary thermal spring west of Māhia Peninsula — are plausibly explained by the existence of deeply subducted seamounts. Plate coupling and shallow SSEs inferred from geodetic observations and inversions also correlate well with the locations of these seamounts. An inferred intraslab fluid source offshore Pōrangahau is imaged below a region of frequent, shallow SSEs and its location is in agreement with previous ideas linking the release of fluid pressure from the downgoing plate with the timing of SSEs.

Based on these findings, we suggest that the upper plate is left extensively fractured in the wake of each subducting seamount, making it less capable than otherwise of storing elastic strain. We propose that upper plate damage can account for the observed differences in along-strike properties of the Hikurangi subduction zone, provides a possible explanation for the locked-to-creeping transition zone and segmentation of shallow SSEs observed, and may mitigate the extent and effects of future large subduction zone earthquakes.

Open Research

The adjoint tomography velocity model analyzed in this study is available through a public repository (https://core.geo.vuw.ac.nz/d/feae69f61ea54f81bee1/). References to data used to derive this velocity model can be found in the following intext citation reference: Chow et al. (companion manuscript).

The authors are in the process of archiving the velocity model on the more permanent public repository: the Incorporated Research Institutions for Seismology Earth Model Collaboration (IRIS EMC).

Acknowledgments

This work was funded by a Rutherford Discovery Fellowship and Marsden Fund awarded by the Royal Society of New Zealand, as well as an Endeavour Fund awarded by the New Zealand Ministry of Business, Innovation and Employment. We thank Laura Wallace, Susan Ellis, and Phil Barnes for helpful discussions.

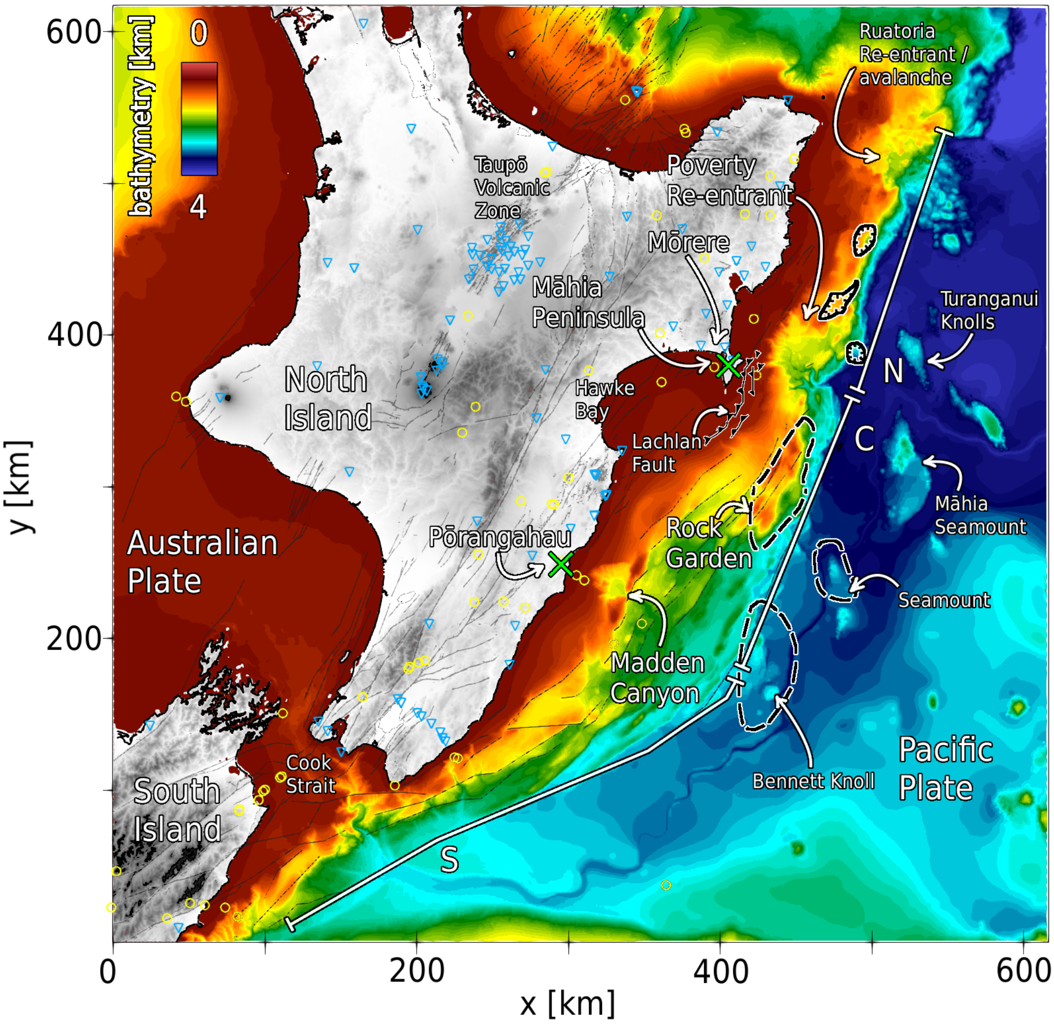

Figure 1. Tectonic setting for the Hikurangi subduction zone offshore New Zealand's North Island. High-resolution bathymetry (Mitchell et al., 2012) highlights the complicated accretionary wedge and numerous seamounts on the incoming Pacific Plate. White solid lines separate the margin into southern (S), central (C), and northern (N) segments. Green crosses show the locations of velocity anomalies below Pōrangahau and Māhia Peninsula. Yellow circles and blue inverted triangles show earthquakes and receivers used to derive the velocity model (Chow et al., companion manuscript). Thin black lines show active faults (Litchfield et al., 2014). Seamounts identified in previous studies are shown with dashed black outlines (Barnes et al., 2010) and solid black outlines (Bell et al., 2010).

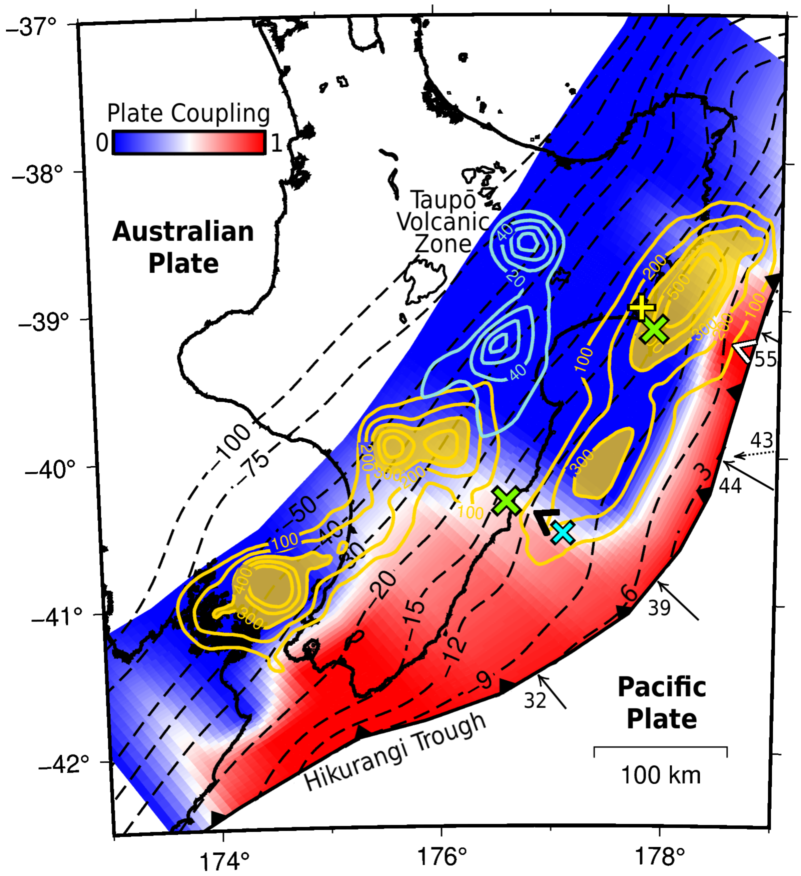

Figure 2. Geophysical setting of the Hikurangi subduction zone. Arrows denote trench-normal convergence rate in units of mm/yr. The dashed arrow shows the plate convergence direction and rate. Colors representing plate coupling coefficient show that the southern Hikurangi margin is effectively locked to 30 km depth (Wallace, Barnes, et al., 2012). Cumulative slow slip events from 2002–2014 shown as yellow and blue contours in units of millimeters. Shaded patches highlight cumulative slip greater than 300 mm. Green X's represent inferred deeply-subducted seamounts. The blue X shows the location of an inferred fluid source in the subducting slab. Black and white "<" markers represent the approximate locations of Madden Canyon and Poverty Re-entrant, respectively. Yellow "+" shows the location of the Mōrere thermal spring, and corresponding geophysical anomalies. Dashed black lines show depth to the plate interface in units of kilometers (Williams et al., 2013).

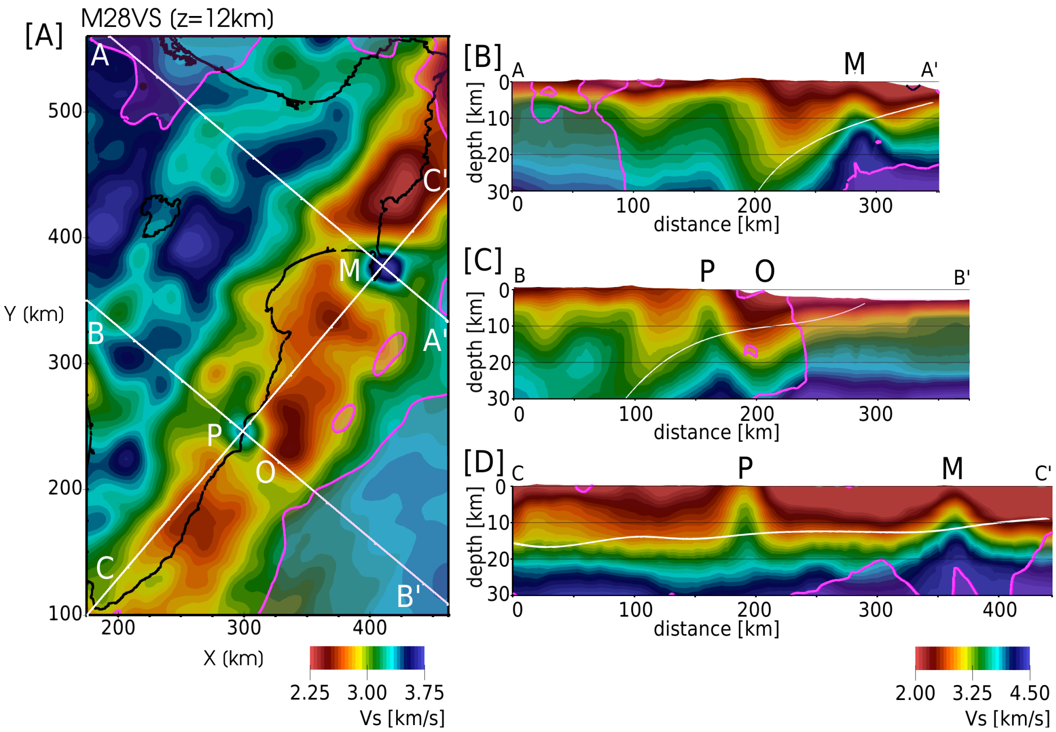

Figure 3. East Coast velocity anomalies shown in V_s. Pink shaded regions highlight the model domain outside the chosen sensitivity threshold, within which model parameters are not interpreted (Figure A1). A) V_s at 12 km depth showing two localized high-velocity anomalies below Pōrangahau (P) and Māhia Peninsula (M), and a broad low-velocity anomaly offshore Pōrangahau (O). Surface traces of cross sections are shown as white lines. B–D) Cross sections through velocity anomalies corresponding to the surface traces shown in A at 3× vertical exaggeration. White line shows plate interface model of Williams et al. (2013).

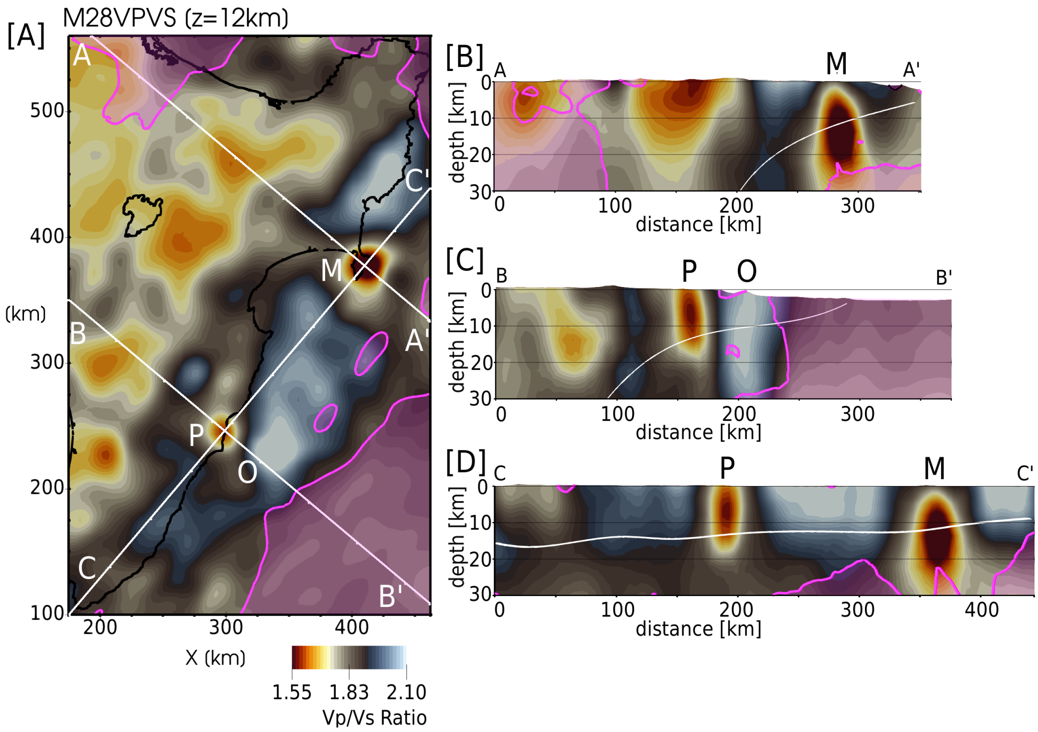

Figure 4. East Coast velocity anomalies in V_p/V_s. Pink shaded regions highlight the model domain outside the chosen sensitivity threshold, within which model parameters are not interpreted (Figure A1). A) V_p/V_s at 12 km depth showing two localized low-V_p/V_s anomalies below Pōrangahau (P) and Māhia Peninsula (M), and a broad highV_p/V_s anomaly offshore Pōrangahau (O). Surface traces of cross sections are shown as white lines. B–D) Cross sections through high-velocity anomalies corresponding to the surface traces shown in A at 3× vertical exaggeration. White line shows plate interface model of Williams et al. (2013).

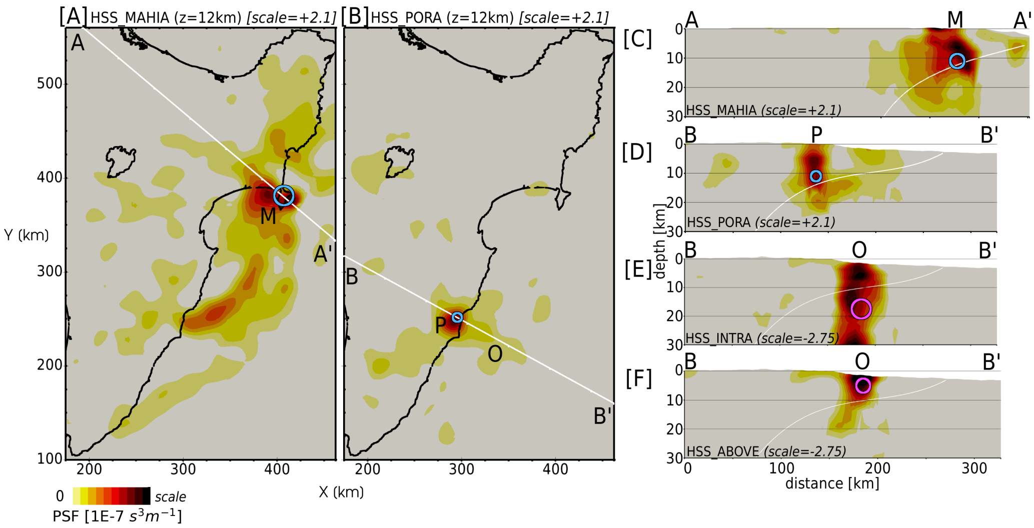

Figure 5. Point spread functions (PSFs) for the Māhia Peninsula (M), Pōranghau (P), and offshore (O) velocity anomalies. Input perturbations are 3D spheroidal Gaussians with peak amplitudes equal to ±15% of the background V_s model. Horizontal (Γ_h) and vertical (Γ_z) full width of the Gaussian perturbations are shown as blue circles for positive perturbations, and pink circles for negative perturbations. A) Māhia Peninsula PSF ($\Gamma_h = 20$ km); A–A' trace shown in panel C. B) Pōrangahau PSF ($\Gamma_h = 10$ km); B–B' trace shown in panels D–F. C) Māhia Peninsula PSF A–A' cross section ($\Gamma_z = 5$ km). D) Pōranghau PSF B–B' cross section ($\Gamma_z = 3.5$ km). E) Intra slab low-velocity anomaly PSF ($\Gamma_{h,z} = 21, 7$ km). F) Above slab low-velocity anomaly PSF ($\Gamma_{h,z} = 15, 5$ km). Note the varying amplitude scale. Cross sections shown at 3× vertical exaggeration. White line in cross sections shows plate interface model of Williams et al. (2013).

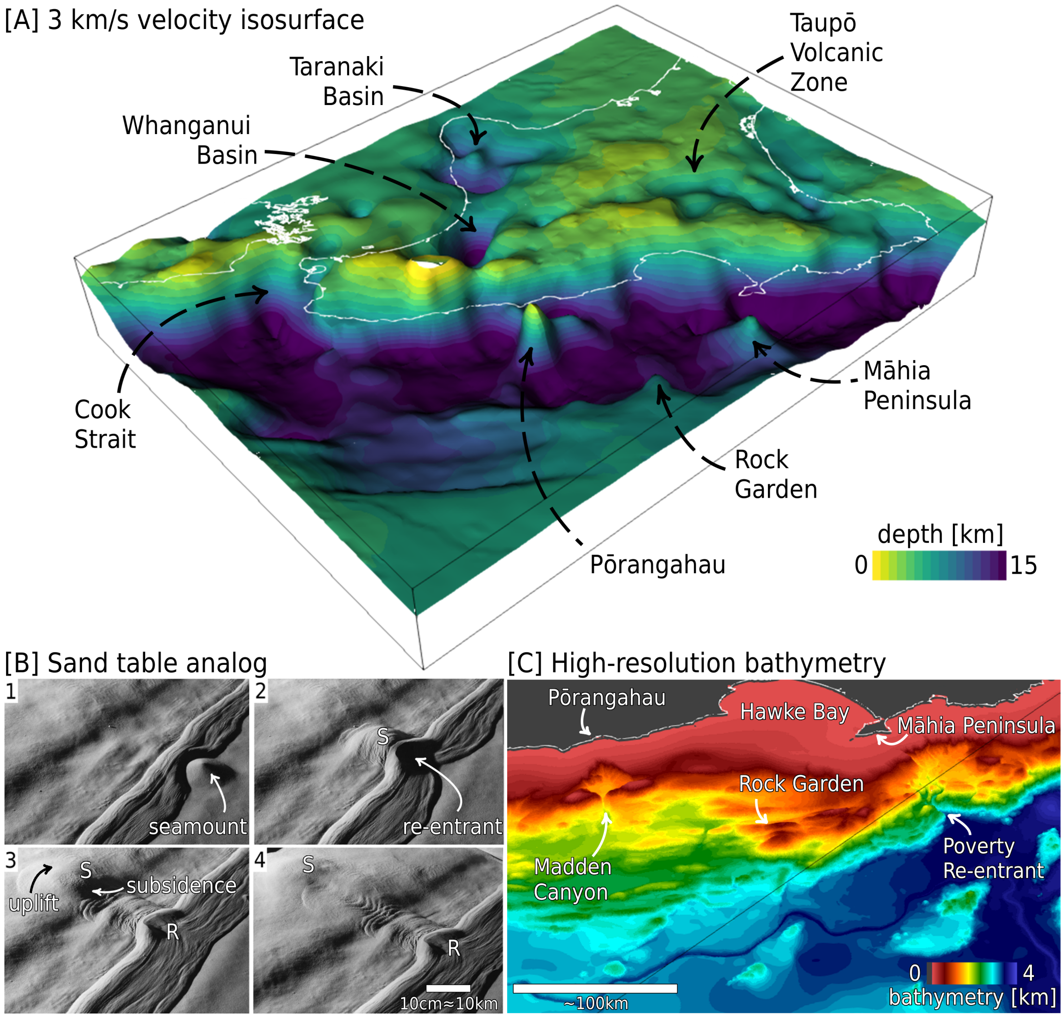

Figure 6. Evidence for deeply subducted seamounts below the East Coast. A) Isosurface for V$_s$=3 km/s colored by depth and vertically exaggerated. Anomalies related to the two inferred seamounts below Pōrangahau and Māhia Peninsula are visible as peaks that likely represent expressions of the seamounts on the upper plate. Also visible is a peaked anomaly related to the known seamount at Rock Garden (C). B) Seamount subduction represented by an analog sand table experiment, modified from Dominguez et al. (1998). Panels represent increasing time: B1) The seamount (S) indents the inner trench slope; B2) A shadow zone forms in the wake of the seamount. The re-entrant (R) is affected by intense mass-sliding; B3) The seamount is subducted further, with local uplift above the seamount, and subsidence in its wake; B4) Extension occurs in the wake of the seamount, leading to a subsided area behind the crest of the seamount. A permanent fracture network is left in the upper plate. C) Offshore East Coast bathymetry showing the relative locations of inferred seamounts and bathymetric features (Mitchell et al., 2012).

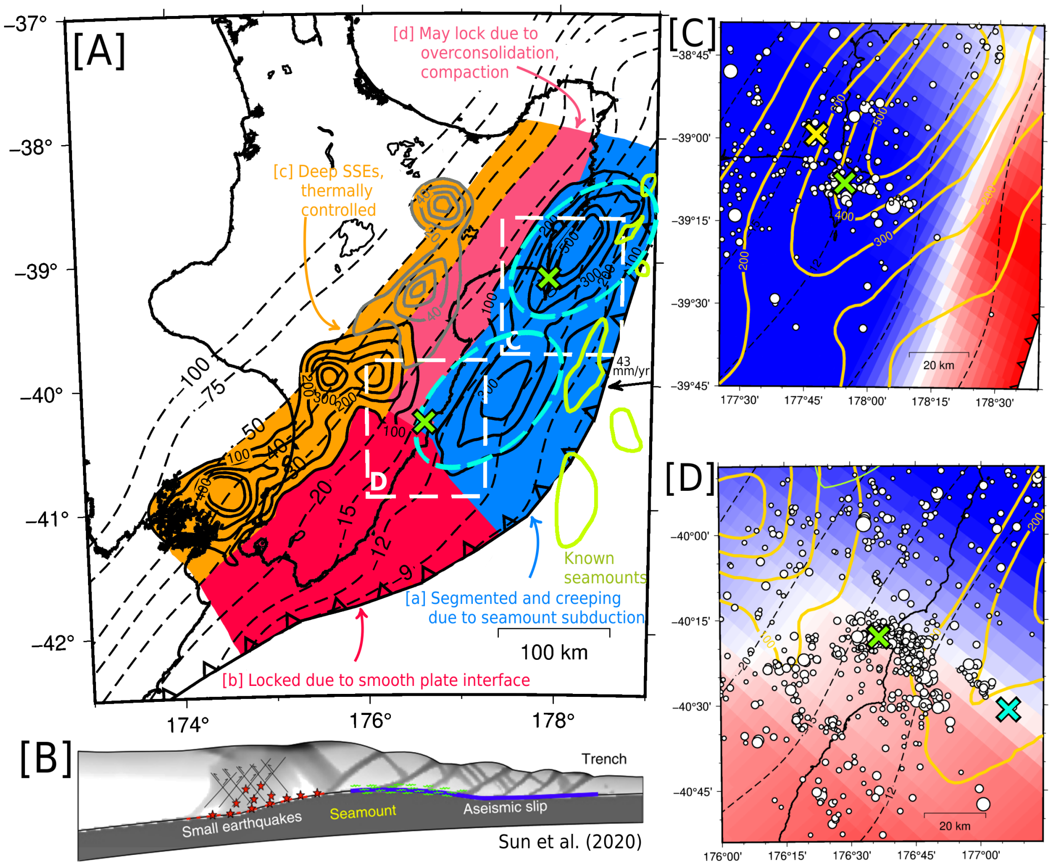

Figure 7. Subducted seamounts (green X's) and seismic and aseismic behavior observed at the Hikurangi subduction margin. A) Possible segmentation of the plate interface, controlled by rough crust subduction at the northern and central Hikurangi margins, in contrast to smooth plate interface at the southern margin. Spatial segmentation of shallow slow slip events highlighted by blue dashed ovals. B) Cartoon cross section of a subduction zone showing expected slip behavior and upper plate faulting during seamount subduction from Sun et al. (2020). C) Māhia Peninsula seamount seismic and aseismic behavior. Earthquakes between 2000 and 2021, M > 2.5 at 1 km below or 4 km above plate interface depths (Williams et al., 2013) shown as white circles. Mōrere thermal spring shown as yellow X. D) Pōrangahau seamount seismic and aseismic behavior. Blue cross shows location of inferred intraslab fluids.

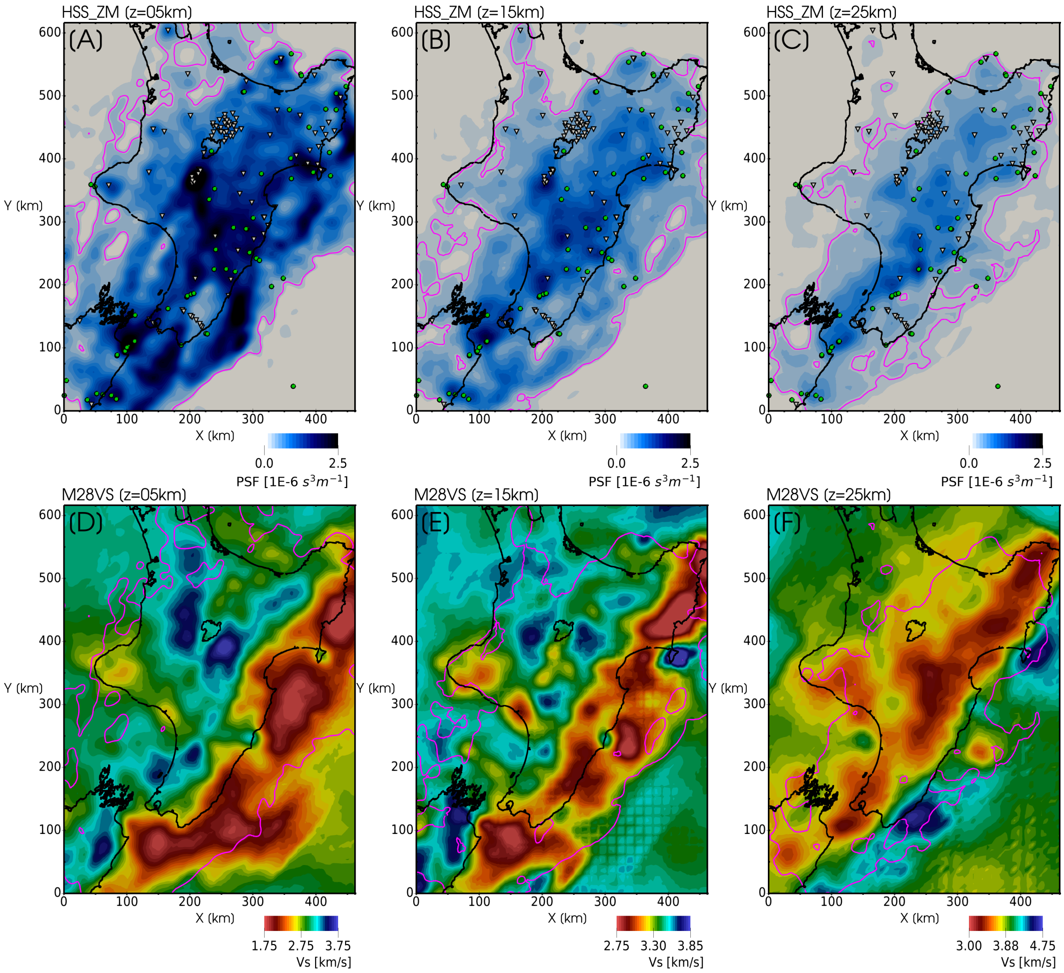

Figure A1. Zeroth moment point spread function (PSF) defining spatial sensitivity of the dataset used to derive our velocity model. The pink line corresponds to a threshold value of $2\text{E}-7\ \text{s}^3\ \text{m}^{-1}$. Velocity heterogeneities located in regions below the threshold have limited to no sensitivity and are consequently not interpreted. A–C) Depth slices through the zeroth moment PSF at 5, 15, and 25 km depth. Green circles and inverted triangles denote sources and receivers used in the inversion, respectively. D–E) Depth slices through our V_s velocity model at 5, 15, and 25 km depth. Pink lines are the same as those shown in A–C.

References

Audet, P., Bostock, M. G., Christensen, N. I., & Peacock, S. M. (2009). Seismic evidence for overpressured subducted oceanic crust and megathrust fault sealing. *Nature*, *457*(7225), 76–78.

Bangs, N. L., Gulick, S. P., & Shipley, T. H. (2006). Seamount subduction erosion in the Nankai Trough and its potential impact on the seismogenic zone. *Geology*, *34*(8), 701–704.

Barker, D., Sutherland, R., Henrys, S., & Bannister, S. (2009). Geometry of the Hikurangi subduction thrust and upper plate, North Island, New Zealand. *Geochemistry, Geophysics, Geosystems*, *10*(2).

Barnes, P. M., Lamarche, G., Bialas, J., Henrys, S., Pecher, I., Netzeband, G. L., ... Crutchley, G. (2010). Tectonic and geological framework for gas hydrates and cold seeps on the Hikurangi subduction margin, New Zealand. *Marine Geology*, *272*(1-4), 26–48.

Barnes, P. M., Nicol, A., & Harrison, T. (2002). Late Cenozoic evolution and earthquake potential of an active listric thrust complex above the Hikurangi subduction zone, New Zealand. *Geological Society of America Bulletin*, *114*(11), 1379–1405.

Beanland, S., & Haines, J. (1998). The kinematics of active deformation in the North Island, New Zealand, determined from geological strain rates. *New Zealand Journal of Geology and Geophysics*, *41*(4), 311–323.

Bell, R., Sutherland, R., Barker, D., Henrys, S., Bannister, S., Wallace, L., & Beavan, J. (2010). Seismic reflection character of the Hikurangi subduction interface, New Zealand, in the region of repeated Gisborne slow slip events. *Geophysical Journal International*, *180*(1), 34–48.

Bozdağ, E., Peter, D., Lefebvre, M., Komatitsch, D., Tromp, J., Hill, J., ... Pugmire, D. (2016). Global adjoint tomography: first-generation model. *Geophysical Journal International*, *207*(3), 1739–1766.

Byrne, D. E., Wang, W.-h., & Davis, D. M. (1993). Mechanical role of backstops in the growth of forearcs. *Tectonics*, *12*(1), 123–144.

Carter, R. M., & Naish, T. R. (1998). A review of Wanganui Basin, New Zealand: global reference section for shallow marine, Plio–Pleistocene (2.5–0 Ma) cyclostratigraphy. *Sedimentary Geology*, *122*(1-4), 37–52.

Chesley, C., Naif, S., Key, K., & Bassett, D. (2021). Fluid-rich subducting topography generates anomalous forearc porosity. *Nature*, *595*(7866), 255–260.

Chow, B., Kaneko, Y., Tape, C., Modrak, R., Mortimer, N., Bannister, S., & Townend, J. (companion manuscript). Strong upper-plate heterogeneity at the Hikurangi subduction margin (North Island, New Zealand) imaged by adjoint tomography. *Journal of Geophysical Research: Solid Earth*.

Chow, B., Kaneko, Y., Tape, C., Modrak, R., & Townend, J. (2020). An automated workflow for adjoint tomography — waveform misfits and synthetic inversions for the North Island, New Zealand. *Geophysical Journal International*, *223*(3), 1461–1480.

Christensen, N. I. (1996). Poisson's ratio and crustal seismology. *Journal of Geophysical Research: Solid Earth*, *101*(B2), 3139–3156.

Collot, J.-Y., Delteil, J., Lewis, K. B., Davy, B., Lamarche, G., Audru, J.-C., ... others (1996). From oblique subduction to intra-continental transpression: Structures of the southern Kermadec-Hikurangi margin from multibeam bathymetry, side-scan sonar and seismic reflection. *Marine Geophysical Researches*, *18*(2), 357–381.

Cummins, P. R., Baba, T., Kodaira, S., & Kaneda, Y. (2002). The 1946 Nankai earthquake and segmentation of the Nankai Trough. *Physics of the Earth and Planetary Interiors*, *132*(1-3), 75–87.

Delahaye, E., Townend, J., Reyners, M., & Rogers, G. (2009). Microseismicity but no tremor accompanying slow slip in the Hikurangi subduction zone, New

Zealand. *Earth and Planetary Science Letters*, *277*(1-2), 21–28.
Dominguez, S., Lallemand, S., Malavieille, J., & von Huene, R. (1998). Upper plate deformation associated with seamount subduction. *Tectonophysics*, *293*(3-4), 207–224.
Dominguez, S., Malavieille, J., & Lallemand, S. E. (2000). Deformation of accretionary wedges in response to seamount subduction: Insights from sandbox experiments. *Tectonics*, *19*(1), 182–196.
Eberhart-Phillips, D., Bannister, S., Reyners, M., & Henrys, S. (2020). *New Zealand Wide model 2.2 seismic velocity and Qs and Qp models for New Zealand [dataset].* Retrieved from `zenodo.org/record/3779523` doi: 10.5281/zenodo.3779523
Eberhart-Phillips, D., Han, D.-H., & Zoback, M. D. (1989). Empirical relationships among seismic velocity, effective pressure, porosity, and clay content in sandstone. *Geophysics*, *54*(1), 82–89.
Eberhart-Phillips, D., Reyners, M., & Bannister, S. (2015). A 3D QP attenuation model for all of New Zealand. *Seismological Research Letters*, *86*(6), 1655–1663.
Eberhart-Phillips, D., Reyners, M., Chadwick, M., & Chiu, J.-M. (2005). Crustal heterogeneity and subduction processes: 3-D Vp, Vp/Vs and Q in the southern North Island, New Zealand. *Geophysical Journal International*, *162*(1), 270–288.
Edbrooke, S., Heron, D., Forsyth, P., & Jongens, R. (2015). *Geological map of New Zealand 1:1 000 000. GNS Science Geological Map 2.*
Ellis, S., Fagereng, A., Barker, D., Henrys, S., Saffer, D., Wallace, L., ... Harris, R. (2015). Fluid budgets along the northern Hikurangi subduction margin, New Zealand: The effect of a subducting seamount on fluid pressure. *Geophysical Journal International*, *202*(1), 277–297.
Fichtner, A., & Trampert, J. (2011). Resolution analysis in full waveform inversion. *Geophysical Journal International*, *187*(3), 1604–1624.
Frederik, M. C., Gulick, S. P., & Miller, J. J. (2020). Effect on Subduction of Deeply Buried Seamounts Offshore of Kodiak Island. *Tectonics*, *39*(7), e2019TC005710.
Heise, W., Caldwell, T. G., Bannister, S., Bertrand, E., Ogawa, Y., Bennie, S., & Ichihara, H. (2017). Mapping subduction interface coupling using magnetotellurics: Hikurangi margin, New Zealand. *Geophysical Research Letters*, *44*(18), 9261–9266.
Hunt, T., & Glover, R. (1995). *Origin of mineral springs on the east coast, North Island, NZ* (Tech. Rep.). Wairakei Research Centre, IGNS, Taupo, NZ.
Ito, H., DeVilbiss, J., & Nur, A. (1979). Compressional and shear waves in saturated rock during water-steam transition. *Journal of Geophysical Research: Solid Earth*, *84*(B9), 4731–4735.
Jacobs, K., Savage, M., & Smith, E. (2016). Quantifying seismicity associated with slow slip events in the Hikurangi margin, New Zealand. *New Zealand Journal of Geology and Geophysics*, *59*(1), 58–69.
King, P. R., & Thrasher, G. P. (1996). *Cretaceous-Cenozoic geology and petroleum systems of the Taranaki Basin, New Zealand* (Vol. 2). Institute of Geological & Nuclear Sciences.
Kodaira, S., Takahashi, N., Nakanishi, A., Miura, S., & Kaneda, Y. (2000). Subducted seamount imaged in the rupture zone of the 1946 Nankaido earthquake. *Science*, *289*(5476), 104–106.
Lewis, K., & Pettinga, J. (1993). The emerging, imbricate frontal wedge of the Hikurangi margin. *Sedimentary Basins of the World*, *2*, 225–250.
Lewis, K. B., Carter, L., & Davey, F. J. (1994). The opening of Cook Strait: interglacial tidal scour and aligning basins at a subduction to transform plate edge. *Marine Geology*, *116*(3-4), 293–312.

Lewis, K. B., Collot, J.-Y., & Lallem, S. E. (1998). The dammed Hikurangi Trough: a channel-fed trench blocked by subducting seamounts and their wake avalanches (New Zealand–France GeodyNZ Project). *Basin Research*, *10*(4), 441–468.

Litchfield, N., Ellis, S., Berryman, K., & Nicol, A. (2007). Insights into subduction-related uplift along the Hikurangi Margin, New Zealand, using numerical modeling. *Journal of Geophysical Research: Earth Surface*, *112*(F2).

Litchfield, N., Van Dissen, R., Sutherland, R., Barnes, P., Cox, S., Norris, R., ... others (2014). A model of active faulting in New Zealand. *New Zealand Journal of Geology and Geophysics*, *57*(1), 32–56.

Marcaillou, B., Collot, J.-Y., Ribodetti, A., d'Acremont, E., Mahamat, A.-A., & Alvarado, A. (2016). Seamount subduction at the North-Ecuadorian convergent margin: Effects on structures, inter-seismic coupling and seismogenesis. *Earth and Planetary Science Letters*, *433*, 146–158.

Mitchell, J. S., Mackay, K. A., Neil, H. L., Mackay, E. J., Pallentin, A., & Notman, P. (2012). *Undersea New Zealand, 1:5,000,000.* Retrieved from `https://niwa.co.nz/our-science/oceans/bathymetry/download-the-data`

Modrak, R., & Tromp, J. (2016). Seismic waveform inversion best practices: regional, global and exploration test cases. *Geophysical Journal International*, *206*(3), 1864–1889.

Mortimer, N. (2004). New Zealand's geological foundations. *Gondwana research*, *7*(1), 261–272.

Nicol, A., Mazengarb, C., Chanier, F., Rait, G., Uruski, C., & Wallace, L. (2007). Tectonic evolution of the active Hikurangi subduction margin, New Zealand, since the Oligocene. *Tectonics*, *26*(4).

Pedley, K. L., Barnes, P. M., Pettinga, J. R., & Lewis, K. B. (2010). Seafloor structural geomorphic evolution of the accretionary frontal wedge in response to seamount subduction, Poverty Indentation, New Zealand. *Marine Geology*, *270*(1-4), 119–138.

Reyes, A., Christenson, B., & Faure, K. (2010). Sources of solutes and heat in low-enthalpy mineral waters and their relation to tectonic setting, New Zealand. *Journal of Volcanology and Geothermal Research*, *192*(3-4), 117–141.

Reyners, M., Eberhart-Phillips, D., & Bannister, S. (2017). Subducting an old subduction zone sideways provides insights into what controls plate coupling. *Earth and Planetary Science Letters*, *466*, 53–61.

Scholz, C. H., & Small, C. (1997). The effect of seamount subduction on seismic coupling. *Geology*, *25*(6), 487–490.

Singh, S. C., Hananto, N., Mukti, M., Robinson, D. P., Das, S., Chauhan, A., ... others (2011). Aseismic zone and earthquake segmentation associated with a deep subducted seamount in Sumatra. *Nature Geoscience*, *4*(5), 308–311.

Sun, T., Saffer, D., & Ellis, S. (2020). Mechanical and hydrological effects of seamount subduction on megathrust stress and slip. *Nature Geoscience*, *13*(3), 249–255.

Tao, K., Grand, S. P., & Niu, F. (2018). Seismic structure of the upper mantle beneath eastern Asia from full waveform seismic tomography. *Geochemistry, Geophysics, Geosystems*, *19*(8), 2732–2763.

Von Huene, R., & Scholl, D. W. (1991). Observations at convergent margins concerning sediment subduction, subduction erosion, and the growth of continental crust. *Reviews of Geophysics*, *29*(3), 279–316.

Wallace, L. (2020). Slow slip events in New Zealand. *Annual Review of Earth and Planetary Sciences*, *48*, 175–203.

Wallace, L., Barnes, P., Beavan, J., Van Dissen, R., Litchfield, N., Mountjoy, J., ... Pondard, N. (2012). The kinematics of a transition from subduction to strike-slip: An example from the central New Zealand plate boundary. *Journal of Geophysical Research: Solid Earth*, *117*(B2).

Wallace, L., Beavan, J., Bannister, S., & Williams, C. (2012). Simultaneous long-term and short-term slow slip events at the Hikurangi subduction margin, New Zealand: Implications for processes that control slow slip event occurrence, duration, and migration. *Journal of Geophysical Research: Solid Earth*, *117*(B11).

Wallace, L., Beavan, J., McCaffrey, R., & Darby, D. (2004). Subduction zone coupling and tectonic block rotations in the North Island, New Zealand. *Journal of Geophysical Research: Solid Earth*, *109*(B12).

Wallace, L., Reyners, M., Cochran, U., Bannister, S., Barnes, P., Berryman, K., ... Power, W. (2009). Characterizing the seismogenic zone of a major plate boundary subduction thrust: Hikurangi Margin, New Zealand. *Geochemistry, Geophysics, Geosystems*, *10*(10). doi: 10.1029/2009GC002610

Wang, K., & Bilek, S. L. (2011). Do subducting seamounts generate or stop large earthquakes? *Geology*, *39*(9), 819–822.

Warren-Smith, E., Fry, B., Wallace, L., Chon, E., Henrys, S., Sheehan, A., ... Lebedev, S. (2019). Episodic stress and fluid pressure cycling in subducting oceanic crust during slow slip. *Nature Geoscience*, *12*(6), 475–481.

Williams, C., Eberhart-Phillips, D., Bannister, S., Barker, D., Henrys, S., Reyners, M., & Sutherland, R. (2013). Revised interface geometry for the Hikurangi subduction zone, New Zealand. *Seismological Research Letters*, *84*(6), 1066–1073.

Wilson, C., Gravley, D., Leonard, G., & Rowland, J. (2009). Volcanism in the central Taupo Volcanic Zone, New Zealand: tempo, styles and controls. *Studies in Volcanology: the Legacy of George Walker. Special Publications of IAVCEI*, *2*, 225–247.

Wilson, C., Houghton, B., McWilliams, M., Lanphere, M., Weaver, S., & Briggs, R. (1995). Volcanic and structural evolution of Taupo Volcanic Zone, New Zealand: a review. *Journal of Volcanology and Geothermal Research*, *68*(1-3), 1–28.

Yang, H., Liu, Y., & Lin, J. (2013). Geometrical effects of a subducted seamount on stopping megathrust ruptures. *Geophysical Research Letters*, *40*(10), 2011–2016.

Zhu, H., Bozdağ, E., & Tromp, J. (2015). Seismic structure of the European upper mantle based on adjoint tomography. *Geophysical Journal International*, *201*(1), 18–52.